Extended Abstracts of the 2009 International Conference on Solid State Devices and Materials, Sendai, 2009, pp444-445

Improved resistive switching of HfO_X/TiN stack with a reactive metal layer and annealing

Pang-Shiu Chen, Heng-Yuan Lee[1,2], Yu-Sheng Chen[1], Frederick Chen[1], and Ming-Jinn Tsai[1]
Department of Chemical and Materials and Engineering, MingShin University of Science & Technology Hsinfong, Hsinchu 304, Taiwan, [1]Industrial Technology Research Institute, Hsinchu 310, Taiwan, [2]Institute of Electronics Engineering, National Tsing Hua University, Hsinchu 300, Taiwan, Phone : 886-3-5593142 ext 3377, Fax : 886-3-5593142, E-mail :pschen@must.edu.tw

1. Introduction

Recently, transition metal oxide-based resistive memory (RM) attracts much attention due to its potential application in the next generation nonvolatile memory (NVM) [1]. Several binary metal oxides with resistance switching (RS) were demonstrated. Low operation voltage and large high/low resistance ratio (R ratio) were the characteristics of these devices [2]. HfO_2 based RM with high resistance suffered non-uniformity of operation parameters, poor endurance, and low device yield [3]. In the previous work, we modified the bipolar resistance switching (BRS) characteristic of HfO_X based RM by using an inserted Ti layer into the anode [4], but the memory cells also showed an issue of wide distribution of high resistance state (HRS). In this study, three reactive metal layers (AlCu, Ti, and Ta) are explored and compared. The results show that a sufficient annealing temperature and a suitable oxygen gettering ability of the reactive metal overlayer can improve the BRS characteristic of the HfO_X films based memory cells.

2. Device Fabrication and measurement

The HfO_X based RM devices in this work were fabricated as followed: A nominal 10 or 20-nm-thick HfO_X film was deposited on TiN bottom electrode (BE)/Ti/SiO_2 above 8 inch Si wafer by ALD system (ASM polygon 8200) at the temperature of 300 °C. Hafnium tetrachloride ($HfCl_4$) and water (H_2O) were used as reactants. The detail of material properties for the HfO_X film can be found elsewhere [4]. The anodic metal, including AlCu, Ti and Ta, were deposited by sputtering methods. A TiN layer was then covered on the prior devices with the reactive metals to avoid further oxidation of these electrodes. A post metal-deposition annealing (PMA) process was also adopted for some of the devices. The distribution of O atoms in the Ti cap layer before and after PMA were revealed by μ-AES. High resolution cross-sectional transmission electron microscopy (HRTEM) was adopted to reveal the microstructure of stack structure with or without PMA. The electrical properties of the memory devices are characterized by HP4156 and HP 4284 LCR meter.

3. Results and Discussion

The dependence of initial current density (J) at 1 V, breakdown voltage (BV), and capacitance for the HfOx devices with a AlCu overlayer on the PMA temperature are shown in Fig. 1 and Fig. 2. With the PMA temperature at 450 °C, the AlCu layer can absorb the oxygen atoms in the buried HfOx layer, which show poor insulator property. The BV of the stack layers show the similar tendency, and the AlCu layer serves as a series resistor. The J and BV in the annealed devices of 500 or 550 °C reduce and increase, respectively. The AlCu layer with high oxygen atoms subjected to enough PMA may be helpful to block the initial leakage current and enhance the BV of the memory. In Fig. 3, the 1st reset I-V curves for the AlCu/HfOx devices with different PMA after the forming step are presented. The devices with a PMA of 500 °C exhibit stable BRS. The as-gown devices or those with PMA of 450 °C do not show RS, which may be due to the permanent damage induced by the forming process. The schematical diagram for the AlCu/HfOx devices subjected to different PMA are shown in Fig 4(a)-(c). The thickness of AlCu overlayer increase after the PMA of 500 °C as shown in Fig 4(d). In Fig. 5, the typical I-V curve of the AlCu RM with stable BRS is observed. The R ratio for this stack RM is ~ 4, and repetitive BRS device with AlCu with 10^4 times of DC switching cycles are observed (not shown here). In Fig. 6, the XTEM of Ti/HfOx stack without or with PMA of 450 °C are shown, the Ti thickness remains the same. The μ-AES analysis indicates that the O atoms in the Ti cap layer increase after PMA. The typical I-V curves for the annealed 10-nm-thick HfOx devices with a Ti or Ta cap layer are depicted in Fig. 7. The Ti/HfOx device with a high R ratio and stable RS is observed. But the set voltage and reset voltage seem to be insensitive on the metal capping layer. Fig. 8 plots the dependence of BV of the Ti memory devices with or without PMA of 450 °C. For the cell size of 0.13 μm^2, the BV of as-grown and annealed device seems the same, which suggests that the Ti layer also serve as a resistor even after PMA of 450 °C. Using a Ti layer, the HfOx memory devices with high R ratio (mostly > 40), robust RW, and high temperature data retention up to 250 °C are observed. The temperature dependence of set and reset voltage in the Ti device are presented in Fig. 9. The voltages of RM with Ti within the measurement temperature range show metal-like and semiconductor-like behavior. The Ti RM devices under high temperature PMA (> 500 °C) do not exhibit any stable RS, which is obviously different with that with a AlCu cap layer. The stable RM devices with a Ta layer also show excellent retention at 85 ad 200 °C as shown in Fig. 10. Compared with the Ti device, the wide distribution of HRS can be improved for the device with a Ta layer (Fig. 11). The standard free energies of the formation metal oxide are plotting in Fig. 12. The formation energy of oxide for these reactive metals play an important role for the improvement of RS of the HfOx RM. Enough reaction between metal (e.g. Ti) and HfOx after PMA may be responsible for high R ratio, and wide HRS distribution of robust HfOx based RM.

4. Conclusions

The modified anode with a reactive metal plays an important role in BRS of the HfO_X based RM followed by a PMA. With AlCu, Ti and Ta as anodic electrode, the HfOx RM cell after an optimal PMA shows improved reliable RS operation, high yield, long endurance, and high temperature retention. The Ti/HfOx RM devices achieve a high R ratio (> 40). With Ta as the cap layer, a tight HRS distribution of RM is observed.

5. References

[1] Z. Wei *et al*., IEDM Tech. Dig., p. 293, 2008. [2] K. M. Kim *et al*. Appl. Phy. Letts 90, 242906, 2007. [3] Seunghyup Lee *et al*. J. ElectroChem Soc. 155, p. H92, 2008. [4] H. Y. Lee *et al*. IEDM Tech. Dig., p. 297, 2008.

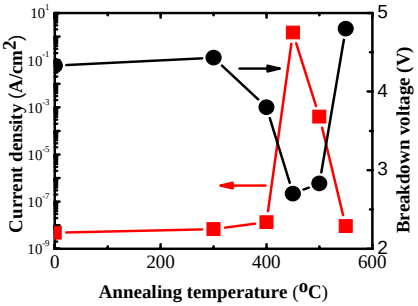

Fig. 1. Dependence of J@1V and BV voltage of AlCu/HfOx devices on PMA.

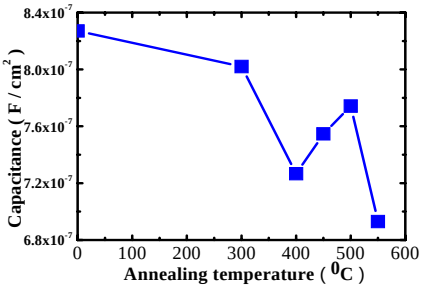

Fig. 2. Dependence of capacitance of TiN/AlCu/HfO/TiN devices on PMA.

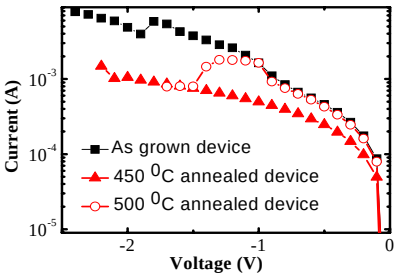

Fig. 3. The 1st reset I-V curves for the AlCu/HfOx devices with different PMA.

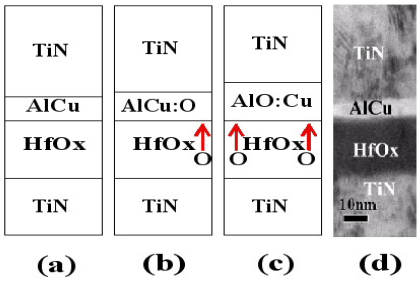

Fig. 4 Schematic to explain proposed mechanism for stack layer: (a) as grown, (b) 450 °C, and (c) 500 °C. In (d), HRTEM of AlCu/HfOx after 500 °C is presented.

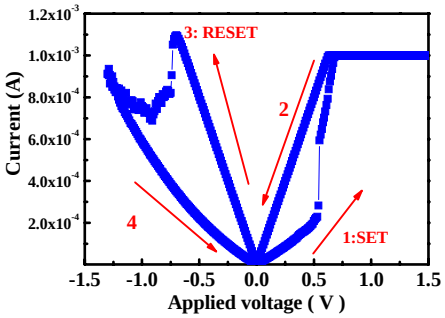

Fig. 5 The typical I-V of stable RW for the AlCu/HfOx devices with PMA of 500 °C.

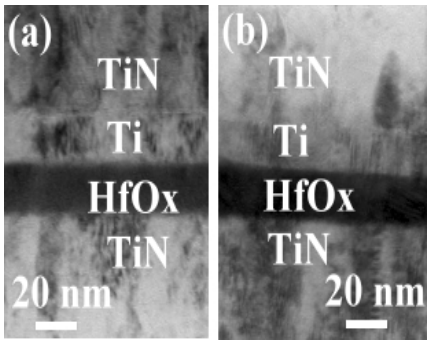

Fig. 6. HRTEM images of Ti/HfOx stack (a) without and (b) with PMA of 500 °C

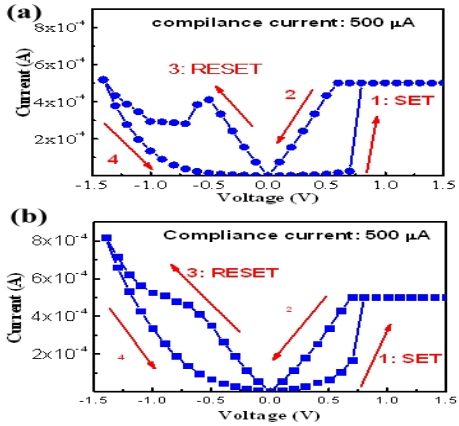

Fig. 7 The I-V curves for the annealed HfOx devices with (a) Ti and (b) Ta layer.

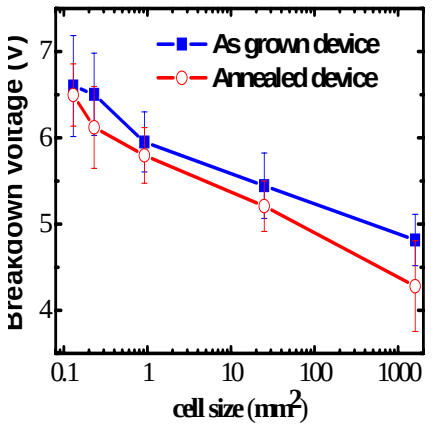

Fig. 8. Dependence of BV of as grown or annealed Ti/HfO devices on the cell size.

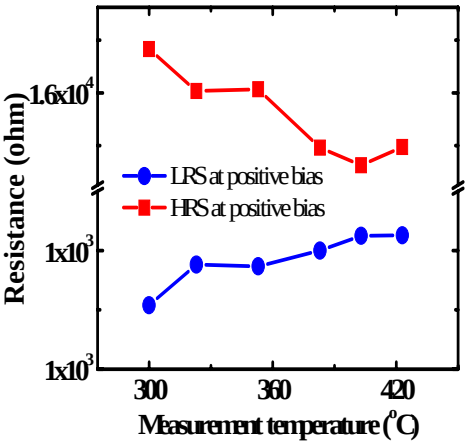

Fig. 9 R_{HIGH} and R_{LOW} of Ti/HfOx devices under different measurement temperature.

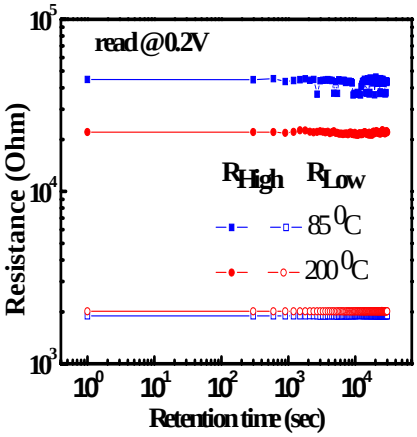

Fig. 10 Data retention for R_{low} and R_{high} for Ta/HfO device at 85 and 200 °C.

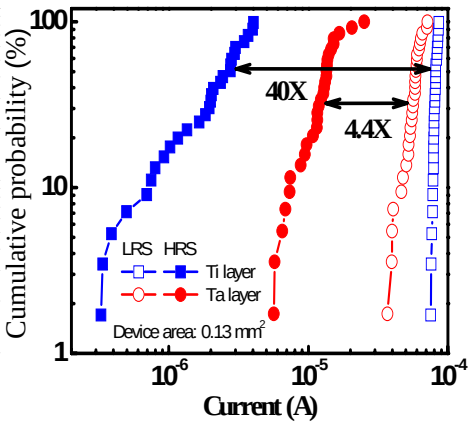

Fig. 11. Resistance distribution for HfOx devices with Ti and Ta layer.

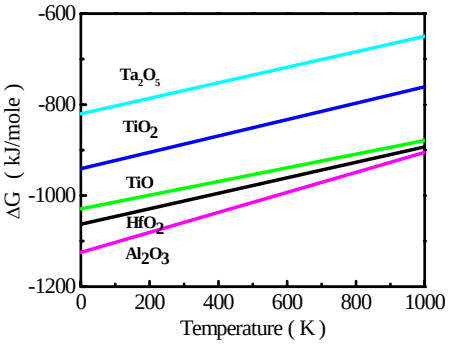

Fig. 12 Ellingham diagram plotting the standard free energies of the formation of oxides (ΔG_o) of the metals mentioned in this work.

Acknowledgement

This work is supported by the National Science Council through Grant No. NSC 97-2221-E-159-018-.